

BCSJ Award Article

Three-Dimensionally Ordered Macroporous (3DOM) Materials of Spinel-Type Mixed Iron Oxides. Synthesis, Structural Characterization, and Formation Mechanism of Inverse Opals with a Skeleton Structure

Masahiro Sadakane,*[1] Chigusa Takahashi,[1] Nobuyasu Kato,[1] Hitoshi Ogihara,[1,2] Yoshinobu Nodasaka,[3] Yoshihiro Doi,[4] Yukio Hinatsu,[4] and Wataru Ueda*[1]

[1]Catalysis Research Center, Hokkaido University, N-21, W-10, Sapporo 001-0021

[2]Japan Society for the Promotion of Science, Chiyoda-ku, Tokyo 102-8472

[3]Laboratory of Electron Microscopy, Graduate School of Dental Medicine, Hokkaido University, Sapporo 060-8586

[4]Division of Chemistry, Graduate School of Science, Hokkaido University, Sapporo 060-0810

Received August 17, 2006; E-mail: sadakane@cat.hokudai.ac.jp

Three-dimensionally ordered macroporous (3DOM) materials of spinel-type MFe_2O_4 (M = Zn, Ni, Zn_xNi_{1-x} ($x = 0.2$–0.8), and Co) mixed iron oxides were prepared in excellent yields by using a colloidal crystal templating method. Mixed metal nitrates were dissolved in an ethylene glycol (EG)–methanol mixed solvent and penetrated into the void of the colloidal crystal template of poly(methyl methacrylate) (PMMA) spheres. During the calcination process, the mixed metal nitrates reacted with ethylene glycol and converted into mixed metal glyoxylate derivatives in the voids of the colloidal crystals before the polymer sphere was removed. After removing the sphere template and converting the mixed metal glyoxylates into the mixed metal oxides, the well-ordered 3DOM materials of the desired spinel-type mixed metal oxides with a skeleton structure were obtained. The preparation procedure was analyzed on the basis of TG-DTA, XRD, SEM, TEM, elemental analysis, and BET surface area determination, and the formation mechanism was clarified. After the PMMA templates were removed, an amorphous 3DOM material with a shell structure was obtained. Crystallization of the amorphous material to the spinel-type mixed metal oxides by further calcination changed the morphology of the 3DOM material from the shell structure to a skeleton structure.

Fabrication of ordered materials in nano-scale order has been one of the most important topics in recent years, and three-dimensionally ordered macroporous (3DOM) materials with pores sized in the sub-micrometer range have become the focus of studies because of their application in photonic crystals, catalysis, and separation.[1] To date almost all of the 3DOM metal oxides have been synthesized by alkoxide-based sol–gel processes: (i) a colloidal crystal template is prepared by ordering mono-disperse spheres, e.g., polystyrene, poly(methyl methacrylate), or silica, into a face-centered close-packed array (opal structure); (ii) interstices in the colloidal crystal are then filled with liquid metal alkoxides, either neat or in solution, which solidify in situ via a sol–gel transformation, resulting in an intermediate composite structure; and (iii) an ordered foam is produced after removing the template by calcinations or extraction. The ordered ("inverse opals") structures synthesized using this method consist of a skeleton surrounding of uniform close-packed macropores. The macropores are interconnected through windows that form as a result of the contact between the template spheres prior to the infiltration of the precursor solution.

However, the alkoxide-based sol–gel method can be applied only to the synthesis of metal oxides (generally, Si, Ti, Zr, and mixture of these), if the metal alkoxide precursor is only moderately reactive. Most of the other metal alkoxides react so quickly that the reaction cannot be controlled. Furthermore, obtaining alkoxide precursors of transition metals and lanthanide metals is difficult and expensive. Commercially available common salts of these metals are usually not suitable for starting materials, because of their melting temperature. These salts melt at a temperature where the template polymer decomposes and, therefore, do not form the 3DOM structure. Solidification of the transition and lanthanide metals before decomposition of the polymer template are necessary.

An elegant method for producing 3DOM materials of the transition-metal oxides has been reported by Stein et al.[2] They infiltrated metal salts (acetate or nitrate) into voids in the colloidal crystals and solidified them as oxalate salts by reacting

Published on the web April 13, 2007; doi:10.1246/bcsj.80.677

the incorporated metal salts with oxalic acid in the voids. The metal oxalate can be converted to metal oxides without melting, which seems to be a key point in successfully producing 3DOM metal oxides (MgO, Cr_2O_3, Mn_2O_3, Fe_2O_3, Co_3O_4, NiO, and ZnO) materials. In other cases, solidification by reacting base, like ammonia[3] or ethylenediaminetetraacetic acid (EDTA),[4] has been reported.

These methods are, however, not suitable for the preparation of 3DOM materials of mixed metal oxides. Each metal has a different reactivity with oxalic acid or base, and the produced oxalate salts or metal hydroxides have different solubility in the reacting media, which causes a mixed metal oxide with an undesired metal ratio.[3a,5] Synthetic procedures that ensure the chemical homogeneity of the product are needed.

Only three methods for producing 3DOM materials of mixed transition or lanthanide metal oxide have been reported to date. 1) 3DOM $Sm_{0.5}Sr_{0.5}CoO_3$ has been prepared from mixed nitrate salts. This is the only example where no solidification is needed.[6] 2) Hur et al. have prepared 3DOM $La_{0.7}Ca_{0.3-x}Sr_xMnO_3$ type perovskite compounds from a mixed metal alkoxide precursor, which is pre-synthesized by reacting their acetate salts with 2-methoxyethanol under acidic conditions.[7] 3) Recently, we have presented a facile one-pot procedure to prepare 3DOM perovskite-type mixed metal oxides, $La_{1-x}Sr_xFeO_3$ ($x = 0$–0.4), which does not need any alkoxide precursor preparation.[8] Our strategy is to use an ethylene glycol (EG)–methanol mixed solution of metal nitrate salts, which are converted to a mixed metal glyoxylate salt by in situ nitrate oxidation at low temperature before the template is removed. Calcination removes the polymer template and causes the conversion of the glyoxylate salt into the mixed metal oxide, i.e., 3DOM perovskite-type materials.

In our last communication,[9] we have reported the preparation of well-ordered 3DOM mixed iron oxides in high yield. In this paper, we describe the synthesis, structural characterization, and formation mechanism of the well-ordered 3DOM spinel-type polycrystalline mixed iron oxide MFe_2O_4 (M = Ni, Zn, Zn_xNi_{1-x} ($x = 0.2$, 0.4, 0.6, and 0.8), and Co) with a skeleton structure in detail. This is the first 3DOM mixed metal oxide containing more than two transition metals in a controlled ratio.

Furthermore, spinel-type mixed iron oxides are technologically important materials because of their magnetic properties, and the nano-scale architecture of the spinel-type mixed iron oxides has recently become a topic of interest. This is the first report, to the best of our knowledge, that the spinel-type mixed iron oxide crystallite can be constructed with a 3DOM architecture.

Experimental

Materials. All chemicals were reagent grade and used as supplied. All metal nitrates were the hydrated form ($Fe(NO_3)_3 \cdot 9H_2O$, $Zn(NO_3)_2 \cdot 6H_2O$, $Ni(NO_3)_2 \cdot 6H_2O$, $Co(NO_3)_2 \cdot 6H_2O$, $Mn(NO_3)_2 \cdot 6H_2O$, and $Cu(NO_3)_2 \cdot 3H_2O$). A suspension (pH 8) of 35 wt % monodisperse polystyrene (PS) spheres with a diameter of 161 ± 10 nm was purchased from Mitsui-Chemicals Inc. Quartz sand (10–15 mesh) was purchased from Kokusan Chemical Works (Tokyo).

Characterizations. Powder X-ray diffraction (XRD) patterns were recorded with a diffractometer (Rigaku, RINT Ultima+) using Cu Kα radiation (tube voltage: 40 kV, tube current: 20 mA) equipped with a graphite monochromator. The diffraction line widths were obtained after the subtraction of the instrumental width determined by the linewidth of a silicon powder sample, and crystallite sizes were calculated from the width of the (311) line using the Scherrer equation. Cell parameters of the ferrite phase were calculated using a least-square method from XRD 11 lines. Images from scanning electron microscopy (SEM) were obtained with a JSM-6300 or JSM-6500F (JEOL) using an accelerating voltage of 5 kV. Samples for SEM were dusted on an adhesive conductive carbon paper attached to a brass mount and were coated with platinum before measurement. Images from transmission electron microscopy (TEM) were obtained with a JEM-2000FX (JEOL) using an accelerating voltage of 200 kV with a LaB_6 filament. Samples for TEM were prepared by sonicating small amounts of the powder in 5 mL of ethanol for 1 min and then depositing a few drops of the suspension on a holey carbon grid. The sonication did not destroy the 3DOM structure. Thermogravimetric-differential thermal analysis (TG-DTA) measurements were performed with a TG-8120 (Rigaku) thermogravimetric analyzer. Nitrogen adsorption measurements were performed on an Autosorb 3 (YUASA IONICS) sorption analyzer. Prior to the sorption measurements, the samples were degassed under vacuum at 573 K for 3 h. Surface areas were calculated by the Brunauer–Emmet–Teller (BET) method. Magnetic measurement was performed using a SQUID (Quantum Design, MPMS-5S). Elemental analyses were performed by the Center for Instrumental Analysis at Hokkaido University.

Synthesis of PMMA Colloidal Crystal Template. Monodisperse poly(methyl methacrylate) (PMMA) spheres (diameter: 291 ± 8 nm) were synthesized by literature techniques and packed into colloidal crystals.[10] Potassium peroxosulfate (1.60 g, 6.0 mmol) and water (720 mL) were stirred at 300 rpm, heated at 353 K, and degassed with flowing argon in a separable four-neck 1000 mL round-bottom flask. After equilibrating to 353 K, methyl methacrylate (MMA) (80 mL, 748 mmol) was poured into the flask, and the resulting suspension was stirred at 353 K for 45 min.

The PMMA colloidal crystal template was prepared by centrifugation (2500 rpm, 1160 G) of the colloidal suspension (ca. 10 g) in a 50 mL centrifugation tube for 2 h. The obtained template was crushed with an agate mortar, and the obtained particles were adjusted into 0.425–2.000 mm using testing sieves (Tokyo Screen, Co., LTD.).

Synthesis of 3DOM Spinel-Type Mixed Metal Oxides. A metal nitrate hydrates mixture (total metal concentration: 2 M) was dissolved with ca. 8 mL of ethyleneglycol (EG) by stirring in a 100 mL beaker at room temperature for 2 h, and the produced EG solution was poured into a 25 mL volumetric flask. Methanol (8 mL) and EG were added in amounts necessary to achieve the desired concentration (the final concentration of methanol was 32 vol %). Then, the PMMA colloidal crystals were soaked in the solution for 2 h. Excess solution was removed from the impregnated PMMA colloidal crystals by vacuum filtration. The obtained sample was allowed to dry in air at room temperature overnight. A 0.5 g amount of the sample was mixed with 2.5 g of quartz sand (10–15 mesh) and calcined in a tubular furnace (inner diameter ca. 12 mm) in an air flow of 50 mL min^{-1}. The temperature was raised at a rate of 1 K min^{-1} to 873 K and held for 5 h.

Synthesis of Non-Porous Spinel Mixed Metal Oxides. The EG–methanol (32 vol %) solution of the mixed metal nitrate (total metal concentration: 2 M) was heated in a muffle oven at a rate of 1 K min^{-1} to 473 K. The produced solid (0.5 g) was calcined in a tube furnace with an air flow of 50 mL min^{-1}. The temperature was raised at a rate of 1 K min^{-1} to 873 K and held for 5 h.

Table 1. Effect of Template Material and Template Size on the 3DOM Fraction

Entry	Template (Diameter/nm)	Fraction of 3DOM /%[a)]
1	PS (160 ± 8)	0
2	PMMA (183 ± 6)	60–70
3	PMMA (291 ± 8)	>90

a) More than 20 particles were randomly chosen by SEM, and the images with magnification of ×5000 to ×10000 were taken. The fraction of 3DOM was calculated as follows; number of particles which contain the 3DOM structure/total number of particles. Calcination condition: heating rate; 1 K min^{-1}, calcination temperature; 873 K (5 h), air flow rate; 50 mL min^{-1}.

Results and Discussion

Synthesis of 3DOM Materials of Spinel-Type Nickel Ferrite ($NiFe_2O_4$); Choice of the Template. In our previous work, we have used PS spheres with a diameter of 161 nm as a template for the preparation of 3 DOM perovskite-type $LaFeO_3$.[8] Our first attempt to produce 3DOM nickel ferrite using PS sphere with a diameter of 161 nm failed. No porous structure could be observed by SEM (Table 1, Entry 1) after the calcination (873 K for 5 h.). By changing the template material from PS to PMMA (particle diameter: 183 nm), the 3DOM structure could be prepared under the same calcination conditions. However, fraction of particles that contained the 3DOM structure was ca. 30% (Table 1, Entry 2). By increasing the template size from 183 to 291 nm, well-ordered 3DOM materials could be obtained in almost all the particles (Table 1, Entry 3). Large fractions (more than 90% of particles by SEM images) of the calcined (at 873 K for 5 h.) sample contained a highly ordered porous structure in three dimensions over a range of tens of micrometers (Fig. S1, Supporting Information). The bigger PMMA template was the best choice for the 3DOM nickel ferrite. Similar template effects have been reported by Stein et al.[5] and Egashira et al.[11] in the case of a monometal system. We decided to use a PMMA colloidal crystal template with a diameter of 291 nm for our research.

Synthesis of 3DOM Materials of Spinel-Type Ferrite (MFe_2O_4, M = Ni, Zn, Co, Cu, Mn, and Zn_xNi_{1-x} (x = 0.2–0.8)). Other 3DOM spinel-type mixed metal ferrites MFe_2O_4 (M = Zn, Co, Cu, and Mn) were prepared using EG–methanol solution of mixed metal nitrates ($M(NO_3)_2 \cdot nH_2O$ ($n = 6$ for Zn, Co, and Mn and $n = 3$ for Cu):$Fe(NO_3)_3 \cdot 9H_2O$ = 1:2; total metal concentration was 2.0 M). The prepared solution was penetrated into the void of the PMMA template (sphere diameter: 291 nm) and calcined at 873 K for 5 h. Powder XRD patterns of the products (Fig. S2, Supporting Information) showed that the desired spinel compound MFe_2O_4 (M = Ni, Zn, Co, and Cu) was obtained, although a solid solution of Mn_2O_3 (JCPDS: 24-0508) + Fe_2O_3 (JCPDS: 39-0238) was obtained in the case of manganese. The production of the desired spinel complexes were confirmed by comparing the calculated lattice parameters from the XRD patterns with reported values in the JCPDS database (Table 2). Furthermore, no metal oxide (NiO, ZnO, CoO, Co_3O_4, or iron oxide) byproduct was observed, indicating that a homogeneous distribution of metal ions was maintained during this procedure. Their SEM images (Fig. 1) showed that well-ordered 3DOM structure was successfully obtained in the case of MFe_2O_4, where M = Ni, Zn, Co, and Zn_xNi_{1-x}, whereas the 3DOM structure of $CuFe_2O_4$ was not obtained (Fig. 1d). In the case of manganese, the 3DOM structure of a solid solution of Mn_2O_3 and Fe_2O_3 was obtained (Fig. 1e). We are not yet sure why 3DOM $CuFe_2O_4$ could not be obtained, but there is one possible explanation. When the calcination was performed at 773 K, the 3DOM structure of mixed phase material ($CuFe_2O_4$, CuO, and Fe_2O_3) was obtained. The phase transformation from the mixed phase to the $CuFe_2O_4$ by increasing the temperature destroyed the 3DOM structure. In the case of the $ZnFe_2O_4$ described in the later section, only one $ZnFe_2O_4$ phase was observed even at 673 K (Fig. S5, Supporting Information).

Table 2. Summary of the Lattice Constants and Crystallite Sizes of MFe_2O_4 (M = Co, Cu, and Zn_xNi_{1-x} (x = 0–1))

Entry	Sample	Crystal system Lattice constant /Å[a),b)]	Crystallite Size/nm
1	$NiFe_2O_4$	8.332 ± 11 (8.339)	17
2	$ZnFe_2O_4$	8.447 ± 11 (8.441)	26
3	$CoFe_2O_4$	8.380 ± 2 (8.377)	24
4	$CuFe_2O_4$	Tetrahedral $a = 5.902 \pm 11$ $c = 8.470 \pm 50$ ($a = 5.844$, $c = 8.630$)	18
5	$Zn_{0.2}Ni_{0.8}Fe_2O_4$	8.370 ± 8	21
6	$Zn_{0.4}Ni_{0.6}Fe_2O_4$	8.378 ± 3	19
7	$Zn_{0.6}Ni_{0.4}Fe_2O_4$	8.399 ± 3	22
8	$Zn_{0.8}Ni_{0.2}Fe_2O_4$	8.418 ± 2	21

a) Lattice constants were calculated from XRD data. b) Values in parentheses were reported value in the JCPDS data 10-0325, 22-1012, 3-0864, and 34-0425 for $NiFe_2O_4$, $ZnFe_2O_4$, $CoFe_2O_4$, and $CuFe_2O_4$, respectively.

This method was successfully applied to the tri-metallic system, and 3DOM $Zn_xNi_{1-x}Fe_2O_4$ mixed spinel ferrites were obtained. As shown in Fig. 1, a well-ordered 3DOM structure was synthesized. XRD of the obtained materials was measured, (Fig. S3, Supporting Information) and the lattice parameters are summarized in Table 2. Although a slight deviation was observed in the case of $x = 0.2$, the lattice parameters increased linearly with an increase in the Zn^{II} ion content (Fig. 2). In other words, a homogeneous distribution of metal ions is maintained with our procedure.[12] This is the most important advantage of our method. Using our method, 3DOM mixed iron oxides could be easily synthesized in the desired metal ratio without using expensive metal alkoxides.

Structural Characterization of 3DOM Spinel-Type Mixed Metal Ferrite. Figure 3 shows enlarged SEM image of the 3DOM $ZnFe_2O_4$. Well-ordered open spheres and interconnected struts created a 3DOM material with a skeleton structure, and the next layer was visible in the SEM images.

The inverse opal structures were classified into three structures, so-called "residual volume structure," "shell structure," and "skeleton structure."[13] The residual volume structure is a perfect inverse opal structure, which can be produced if the whole space among the opal spheres is completely filled by the

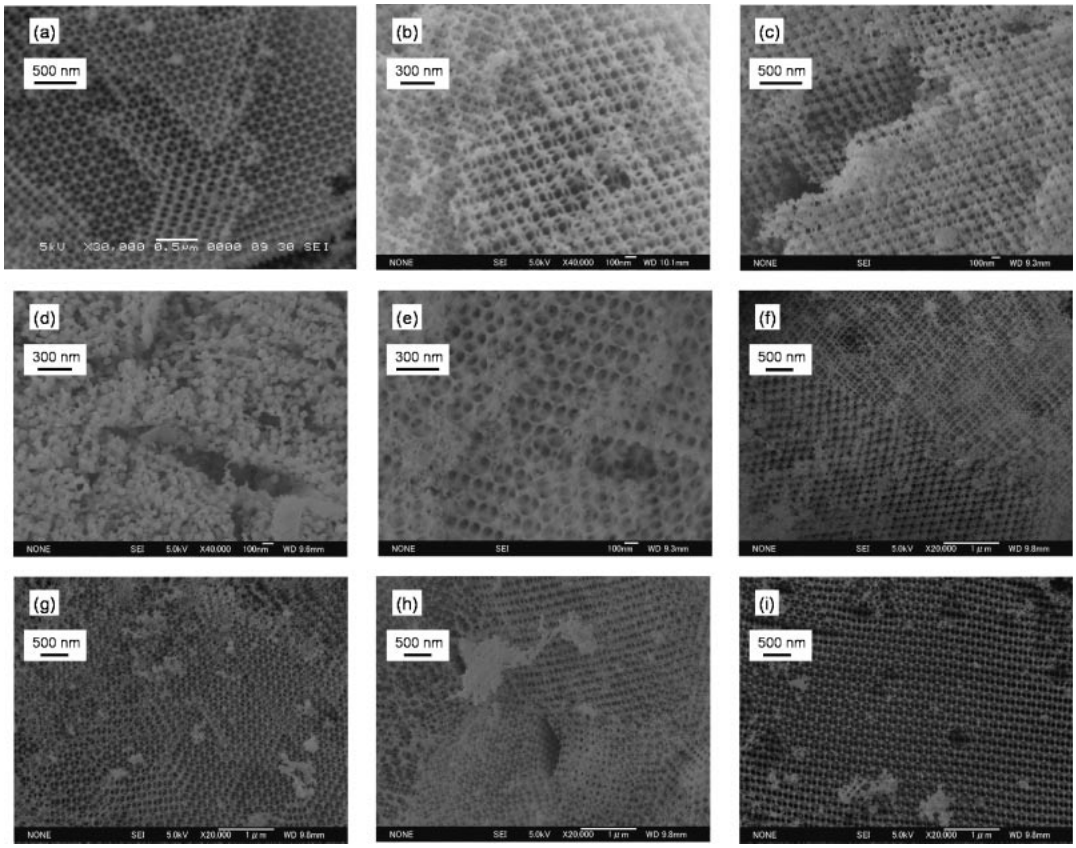

Fig. 1. SEM images of solid materials obtained after calcination at 873 K of PMMA (diameter: 291 nm) colloidal crystal infiltrated by EG–methanol (32 vol %) mixed solution of $M(NO_3)_2$ and $Fe(NO_3)_3$ (M:Fe = 1:2, total metal concentration: 2 M) M = Ni (a), Zn (b), Co (c), Cu (d), Mn (e), $Zn_{0.2}Ni_{0.8}$ (f), $Zn_{0.4}Ni_{0.6}$ (g), $Zn_{0.6}Ni_{0.4}$ (h), and $Zn_{0.8}Ni_{0.2}$ (i). Calcination rate was 1 K min^{-1}, and the calcination temperature was maintained for 5 h.

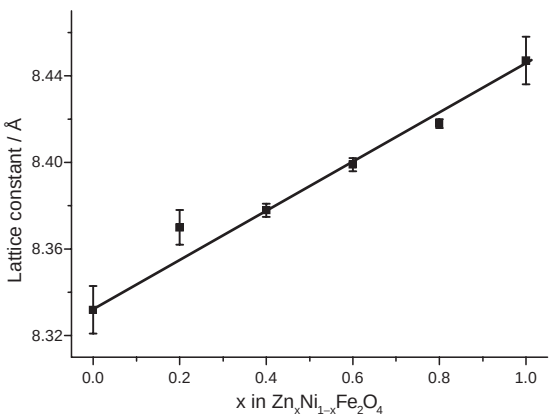

Fig. 2. Variation of lattice constant a vs Zn^{II} content for $Zn_xNi_{1-x}Fe_2O_4$.

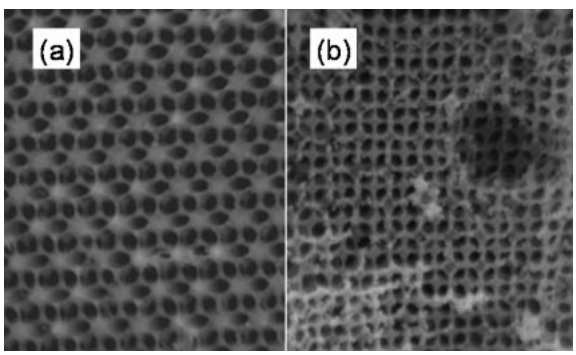

Fig. 3. SEM images of the 3DOM $ZnFe_2O_4$. View toward (111) plane (a) and view toward (100) plane (b). Calcination temperature was 873 K.

product materials.[14] If the space is incompletely filled, the surface of the sphere templates is covered by the product materials, and the shell structure is generated.[15] Most amorphous compounds tend to form the shell structure. On the other hand, crystal compounds tend to form the skeleton structure. The skeleton structures of NiO,[2] Co_2O_3,[2] ZrO_2,[16] TiO_2,[13,17] Ni,[5a] Fe,[5a] Fe_2O_3,[17] and Al_2O_3[3c] have been reported. However, none of these reports have described the formation mechanism in detail.

The skeleton structure consists of strut-like bonds and vertices, with the struts connecting two kinds of vertices. The two vertices are replicas of the former octahedral and tetrahedral voids of the opal structure. These struts and vertices form a CaF_2 lattice, where the 8-coordinated square prism calcium (the former octahedral voids of the opal) vertex is bigger than the tetrahedral fluorine (the former tetrahedral voids of the opal) vertex.[18] A model of the skeleton structure is depicted in Fig. 4. The view towards (111), (100), and (110) plane of the skeleton structure presents the hexagonal, square, and lozenge arrangements, respectively, as shown in Figs. 4b, 4c, and 4d.

As seen in Figs. 5a and 5b, the width of the struts (20–30 nm) and the grain sizes were similar to the crystallite size calculated by Scherrer's equation from XRD data (Table 2 Entry 2 or Table 3 Entry 7), indicating the grains seen in Fig. 5b are the crystallites. Straight connections of the crystallites make the strut-like bonds, and agglomerations of the crystallites make the vertices. The struts connect the tetragonal and square prism vertices (marked as t and s, respectively, in Fig. 5a) one after the other to produce an inverse opal structure. Continuous ordering of the inverse opal structure was confirmed by observing the hexagonal, square, and lozenge arrangement of the (111), (100), and (110) planes, as shown in Figs. 5c–5e, respectively. In the view toward (100) plane (Fig. 5c), long range order (ca. 3 μm long) of the small tetragonal vertexes and big square prism vertices were observed one after the other in the square arrangement could be observed.

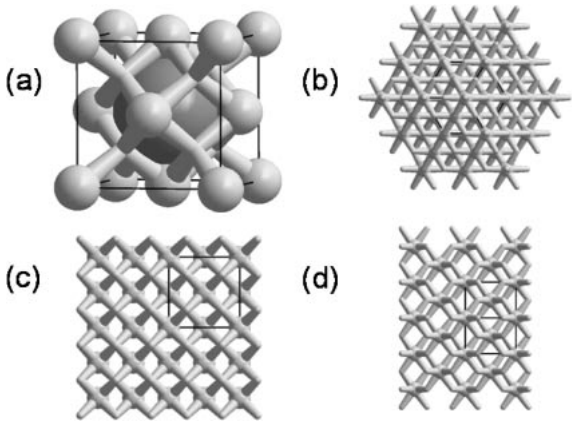

Fig. 4. Model of the inverse opals with skeleton structure: cubic unit cell with a lattice constant *a*, the dark gray ball in the center represents the template sphere (a); view toward (111) plane (b); view toward (100) plane (c); view toward (110) plane (d). In the model, the diameters of the tetrahedral and square prism vertexes were 0.12*a* and 0.31*a*, respectively, using Diamond Version 3.1a (copyright Crystal Impact GbR).

Average pore size of 183 ± 4 nm corresponding to a distance between the centers of two neighboring open spheres was estimated from TEM images (Fig. 5f). This value corresponded to 63% of shrinkage from the original PMMA sphere. This shrinkage was caused by melting of the PMMA spheres and sintering of the produced $ZnFe_2O_4$. This shrinkage will be discussed in detail in the next section. The pore was surrounded by 12 rhombic windows (rhombic dodecahedron), and the long diagonal distance and short diagonal distance of the window were estimated to be 102 and 87 nm, respectively (Fig. 5f).

The non-porous materials prepared without template at the calcination temperature of 873 K had a similar crystallite size (26 nm) and smaller surface areas ($23\ m^2\ g^{-1}$) compared to porous materials ($27\ m^2\ g^{-1}$, Table 3 Entry 6). These values are smaller than the surface area calculated from the crystallite size ($43\ m^2\ g^{-1}$)[19] due to contact of the crytallites. The material produced without the templates was a closed agglomerate of polycrystallites (Fig. S4, Supporting Information) and had more contact compared to the 3DOM materials, causing a slightly smaller BET surface area. A similar small increase of the BET surface area was observed in the case of 3DOM $LaFeO_3$.[8]

Formation Mechanism of the 3DOM Spinel-Type Mixed Metal Ferrite. The calcination process was first analyzed by TG-DTA. TG-DTA curves of a EG–methanol solution containing $Zn(NO_3)_2 \cdot 6H_2O$ and $Fe(NO_3)_3 \cdot 9H_2O$ (total metal concentration: 2 M) without a polymer template is shown in Fig. 6a. Weight loss from room temperature to ca. 340 K with an endothermic DTA peak corresponds to methanol and H_2O evaporation. Sudden weight loss around ca. 340 K with exothermic peak was observed. This weight loss corresponds to the reaction of EG with metal nitrate to produce metal gly-

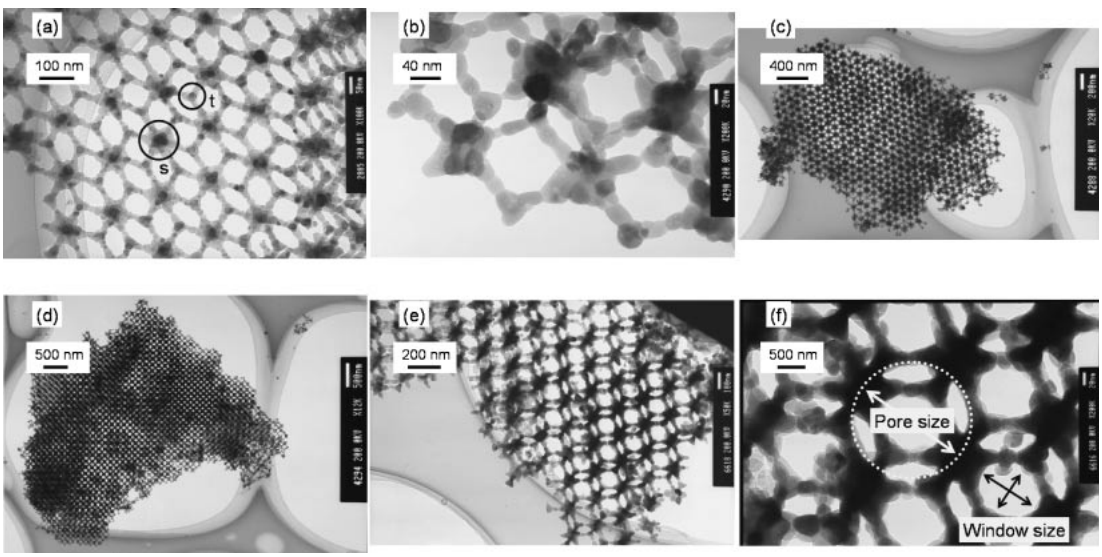

Fig. 5. TEM images of the $ZnFe_2O_4$ material. $\times 100 \times 10^3$ (a), $\times 200 \times 10^3$ (b), $\times 20 \times 10^3$; view toward (111) plane (c), $\times 12 \times 10^3$; view toward (100) plane (d), $\times 50 \times 10^3$; view toward (110) plane (e), enlarged $\times 200 \times 10^3$ of e (f). In part (a), a tetrahedral vertex and 8-coordinated square prism vertex were marked as t and s, respectively.

Table 3. Summary of the Calcination Conditions and Physicochemical Properties Prepared at Different Calcination Temperatures for the Preparation of 3DOM $ZnFe_2O_4$

Entry	Calcination temp/K	BET surface area/$m^2\ g^{-1}$	Crystallite size/nm[a)]	Pore size /nm[b)]	Window size/nm[b)]	Elemental analysis/wt %			
						C	N	H	S
1	473[c)]	n. d.	n. d.	192 ± 9	n. d.	54.7	0	7.3	<0.2
2	473	n. d.	n. d.	n. d.	n. d.	52.3	0	7.0	<0.2
3	573	77	n. d.	198 ± 8	$71 \pm 8 \times 67 \pm 5$	2.4	0	0.6	0.3
4	673	63	13	203 ± 5	$59 \pm 10 \times 56 \pm 9$	1.6	0	0.5	0.3
5	773	38	15	185 ± 4	$76 \pm 6 \times 71 \pm 6$	0	0	0.3	0.3
6	873	27	26	183 ± 4	$102 \pm 7 \times 87 \pm 4$	0	0	0.2	0.2
7	973	21	35	—	—	0	0	0.2	0.2
8	1073	8	46	—	—	0	0	0.2	0.2

a) Crystallite sizes were calculated from the width of the (311) line using the Scherrer equation corrected for instrumental broadening. b) Pore sizes corresponding to the distance between the centers of two neighboring open spheres and window sizes were averaged over 20 pore sizes estimated by (110) direction of TEM images. Conditions: air flow (50 mL min^{-1}), heating rate (1 K min^{-1}), the calcination temperature was kept for 5 h. c) The heating was stopped immediately after reaching the calcination temperature.

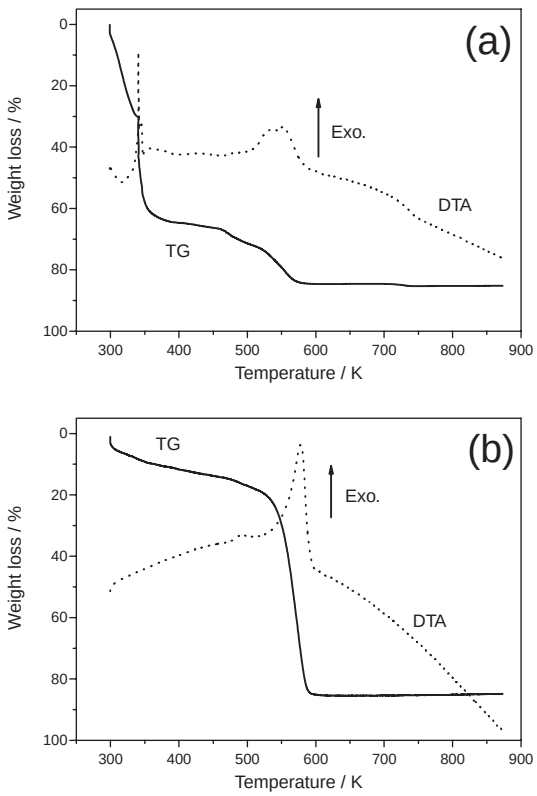

Fig. 6. TG-DTA curves of EG solution of $Zn(NO_3)_2$ and $Fe(NO_3)_3$ (total metal concentration: 2 M) at heating rate of 1 K min^{-1} (a) and PMMA filled with EG–methanol (32 vol %) mixed solution of $Zn(NO_3)_2$ and $Fe(NO_3)_3$ (total metal concentration: 2 M) (b) at heating rate of 1 K min^{-1}. Air flow rate was 30 mL min^{-1}.

oxylate ($[C_2H_2O_4]^{2-}$) or oxalate ($[C_2O_4]^{2-}$) and NO_x gas. The small weight loss at around 370 K corresponds to the evaporation of the remaining H_2O produced by the nitrate oxidation and present in the solution of the metal nitrate hydrate. Stefanscu et al. have reported a similar reaction in aqueous media,[20] and we have reported a similar reaction for the synthesis of 3DOM $LaFeO_3$.[8] The small weight loss around 470 K corresponds to the evaporation of the remaining EG (the boiling point of EG is 470 K). The weight loss up to 510 K was ca. 72%, indicating the presence of the desired $ZnFe_2$-glyoxylate.[21] We also heated the solution in an oil bath and observed brown gas evolution (the color of NO_x) at around 348 K. The weight decrease continued up to ca. 750 K with a total weight loss of 86%, indicating the presence of $ZnFe_2O_4$.[21] The production of the $ZnFe_2O_4$ was also confirmed by XRD of the solid material obtained by calcination at 873 K of the solution. Figure 6b shows TG-DTA chart of the EG–methanol solution containing $Zn(NO_3)_2$ and $Fe(NO_3)_3$ (total metal concentration: 2 M) infiltrated in PMMA. The weight loss up to ca. 500 K corresponded to the evaporation of the methanol, the NO_x, and the remaining EG. The big weight loss between 500 and 600 K with an exothermal peak corresponded to the oxidative decomposition of PMMA and $ZnFe_2(C_2H_2O_4)_4$. TG-DTA chart of the PMMA under the same condition is shown in Fig. S5a (Supporting Information). The solidification (glyoxylate formation) temperature is below the oxidative degradation temperature of PMMA, which is crucial for the formation of well-ordered 3DOM materials.

In order to confirm the formation mechanism more in more detail, products prepared in the temperature range of 473 to 1073 K with a heating rate of 100 K were characterized by elemental analysis, XRD, TEM, and BET surface area analysis, and the results are summarized in Table 3. In the elemental analysis of the products, no nitrogen was observed in the product obtained at a calcination temperature of 473 K, indicating the nitrate oxidation was complete up to 473 K, which was consistent with TG-DTA analysis.[22] Carbon contents remained up to 473 K and decreased suddenly at 573 K. No carbon was detected at 773 K, which was coincident with TG-DTA analysis. A very small amount of sulfur (near detection limit) was detected in the materials prepared between 573 and 1073 K. Sulfur was present in the PMMA template because it was synthesized using $K_2S_2O_8$ as a polymerization initiator. To remove this sulfur, a calcination temperature of more than 1173 K was needed.

Powder XRD patterns of the products calcined at 573, 673, 773, 873, 973, and 1073 K are shown in Fig. S6 (Supporting Information). A calcination temperature of more than 773 K

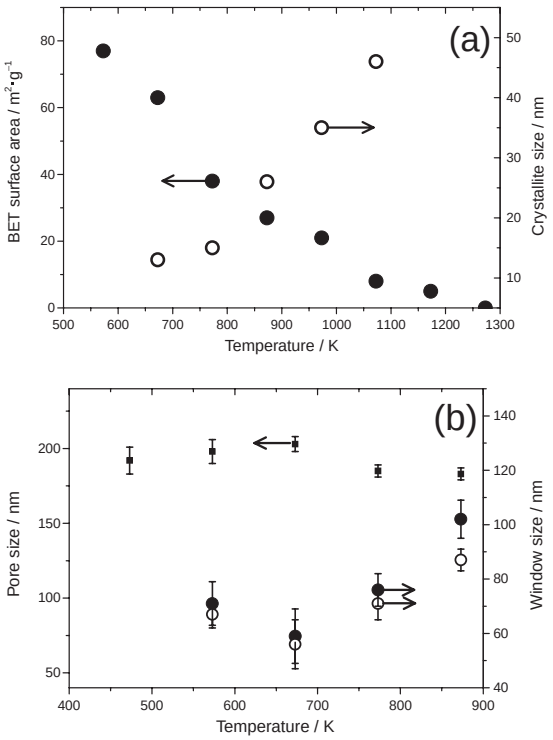

Fig. 7. Temperature effect on BET surface area and crystallite size (a) and pore size and window size (b).

was necessary to produce the desired $ZnFe_2O_4$ mixed metal oxide phase (Fig. S6c, Supporting Information). The product calcined up to 673 K was an amorphous compound (Figs. S6a and S6b). High BET surface area of the material (Table 3, Entry 3) obtained for the product calcined at 573 K was due to the amorphous nature of the product and the remaining carbon. Increasing of the calcination temperature increased the crystallite sizes and decreased the BET surface areas (Fig. 7a).

Figure 8 shows TEM images of the products calcined at 473, 573, 673, 773, 873, 973, and 1073 K. Up to 873 K, 3DOM structure was observed, and it collapsed at 973 K. PMMA polymer could be seen (Figs. 8a and 8b) in the sample obtained at 473 K, which is consistent with TG-DTA and elemental analysis results. Average pore sizes decreased from the initial PMMA sphere diameter (291 nm) to ca. 192–203 nm for calcination temperature between 473 and 673 K (Table 3, Entries 1, 3, 4, and 5, Fig. 7b) where amorphous products were detected by XRD. Furthermore, the "shell structure" was observed in the amorphous 3DOM materials, and additional pores in the square prism vertices were clearly seen in the images toward (100) direction (Figs. 8e and 8h). The pores in the square prism vertices were even observed in the image toward (110) direction (Fig. 8c), when the sample prepared at 473 K was fixed in epoxy glue and sliced using a microtome. Inner pores in the tetragonal vertex could not be observed because both the tetragonal vertices were smaller than the square prism vertices and the tetrahedral arrangement of the struts made it difficult to observe the inner pore. Crystallization changed the "shell structure" to the "skeleton structure," but did not cause much of a decrease in the pore size (Table 3, Entries 5 and 6), and the pore sizes of the polycrystalline 3DOM $ZnFe_2O_4$ was ca. 183–185 nm (Fig. 7b). The window shape of the amorphous $ZnFe_2O_4$ was circular, which corresponded to the shape formed when two PMMA spheres touch each other, as shown in Figs. 8c, 8f, and 8i. Crystal growth increased the window sizes anisotropically, and the shape changed from circle to rhombic (Fig. 7b). The pores in the square prism vertexes still existed in the sample prepared at 873 K (Figs. 3b and 8n).

Most of the shrinkage of the pore occurred below 473 K. SEM images of PMMA (the diameter was 291 nm) heated at 323, 373, 423, and 473 K are shown in Fig. S7 (Supporting Information). The diameter did not change up to 373 K, but decreased to 226 ± 13 nm at 423 K. The sphere disappeared at 473 K. Above the glass-transition temperature (our PMMA, ca. 400 K, Fig. S5b), the viscosity of the PMMA drastically decreased, and the PMMA sphere melted, which decreased the sphere size. Shrinkage of the 3DOM materials from the original polymer spheres has been reported.[1a] Stein et al. have reported a similar shrinkage of crystalline NiO material due to shrinkage of polymer latexes and shrinkage of the wall as the crystal grows.[2]

High yield of the 3DOM material was achieved by adding of methanol to the EG solution. When we used an EG solution, the fraction having the desired 3DOM structured fraction was reduced, and addition of methanol increased the fraction of particles having the 3DOM structure. PMMA shrinkage squeezed the precursors out of the template void, and further calcination of the precursor outside of the template produced nonporous materials. Methanol was easily removed from the template void due to its low boiling point (338 K). The removal of the methanol made a space in the void, and the amount of the precursor squeezed out of the template decreased. Therefore, the fraction of the 3DOM structure increased by using EG–methanol mixed solvent.

The formation mechanism is summarized in Scheme 1. Mixed iron nitrates react with EG to produce the a mixed iron glyoxylate or oxalate salt in the void of the template spheres at a low temperature before the PMMA template melts. Melting of the PMMA reduces the pore size. Evaporation of methanol and the remaining EG produce the open space in the void (shell structure). Further heating causes oxidative removal of the PMMA and converts the mixed iron glyoxylate derivatives into the desired spinel-type mixed iron oxides. Crystallite growth changes the 3DOM material from the "shell structure" to the "skeleton structure," and well-ordered 3DOM spinel-type mixed iron oxide with skeleton structure are formed.

Conclusion

Well-ordered 3DOM spinel-type $M_2Fe_2O_4$ (M = Ni, Zn, Co, and Zn_xNi_{1-x} ($x = 0.2$, 0.4, 0.6, and 0.8)) mixed metal oxide were successfully prepared using an EG–methanol solution of mixed iron nitrate infiltrated PMMA colloidal crystal template in high yield. More than 90% of the obtained materials had the 3DOM structure. The crystallites of the spinel-type mixed iron oxide formed struts and tetrahedral and square prism vertices. The struts connect the tetrahedral and square prism vertices to produce inverse opals with skeleton structure in three dimensions. This is the first example of the spinel-type mixed metal oxide crystallites that have an inverse opal structure. The formation mechanism was clarified. Together with

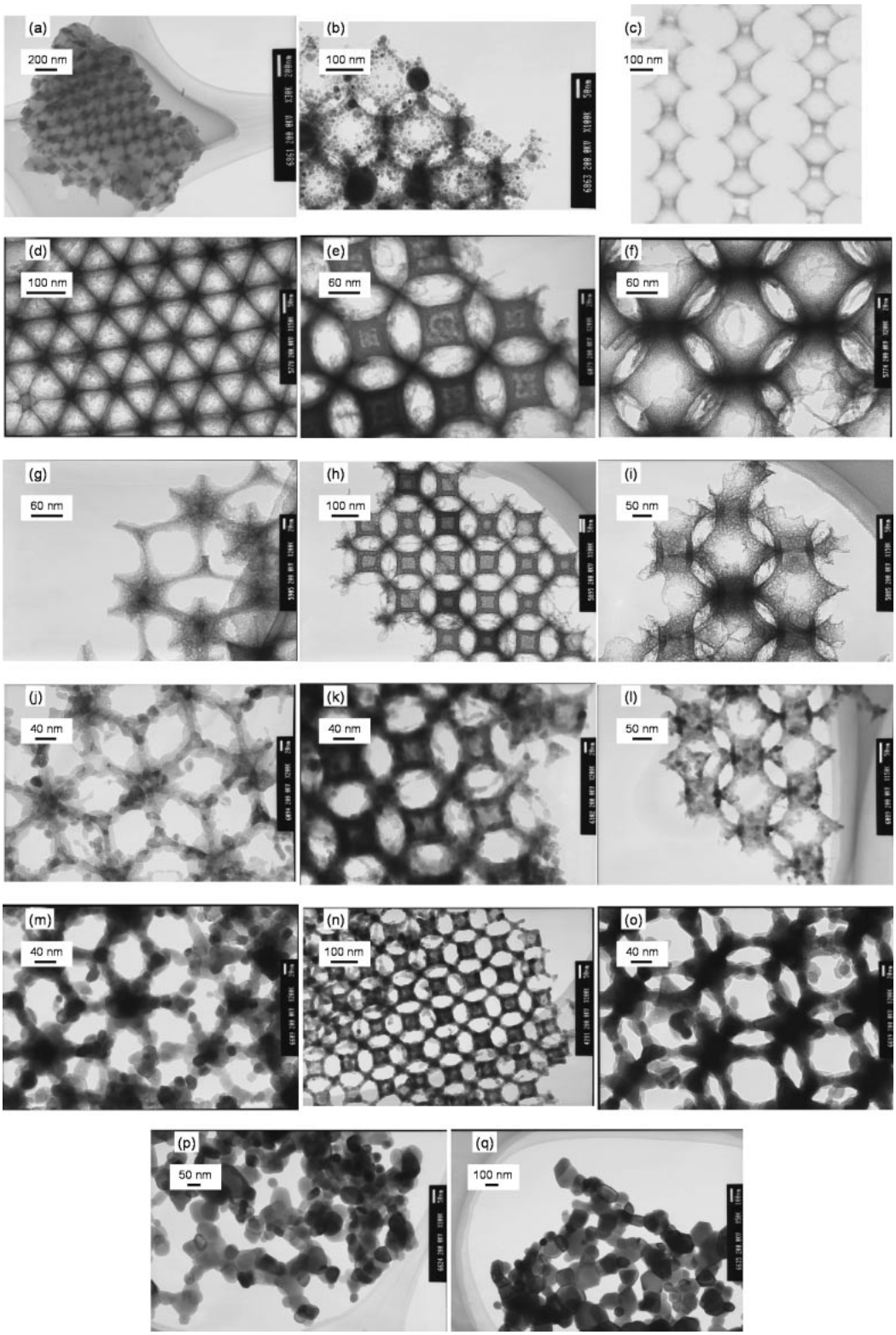

Fig. 8. TEM images of $ZnFe_2O_4$ materials. Prepared at 473 K (a)–(c), 573 K (d)–(f), 673 K (g)–(i), 773 K (j)–(l), 873 K (m)–(o), 973 K (p), and 1073 K (q). View toward (111) plane (d), (g), (j), and (m). View toward (100) plane (e), (h), (k), and (n). View toward (110) plane (b), (c), (f), (i), (l), and (o). The sample was fixed in epoxy glue and sliced (c).

our previous papers,[8,9] we demonstrated that our method is a versatile method for preparing various 3DOM mixed iron oxides. Further application of these materials is now being investigating.[23]

We would like to thank Mr. Kenji Sugawara (High Voltage Electron Microscope Laboratory, Center for Advanced Research of Energy Conversion Materials, Hokkaido University) for running TEM measurement and Mr. Toshitaka Horiuchi

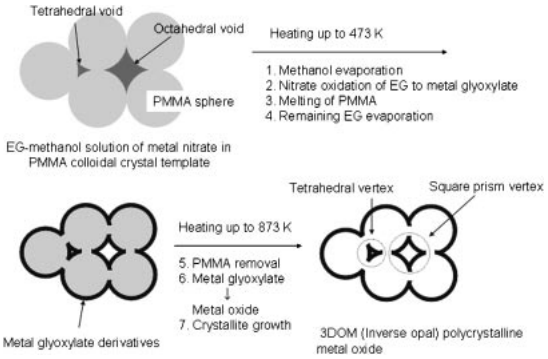

Scheme 1. Formation mechanism of the 3DOM polycrystalline metal oxide.

for his assistance. We would like to thank Grants-in-Aid for Scientific Research (Scientific Research "B," No. 18360383) for financial support. M. S. would like to thank Northern Advancement Center for Science and Technology (NOASTEC) and Hokkaido University Grant Program for supporting young researchers with financial support.

Supporting Information

SEM images of $NiFe_2O_4$ and $ZnFe_2O_4$ (Fig. S1), XRD of 3DOM MFe_2O_4 (M = Ni, Zn, Co, Cu, and Mn) (Fig. S2), XRD of 3DOM $Zn_xNi_{1-x}Fe_2O_4$ ($x = 0.2$, 0.4, 0.6, and 0.8) (Fig. S3), TEM image of non-porous $ZnFe_2O_4$ (Fig. S4), TG-DTA curves of PMMA (Fig. S5), XRD of 3DOM $ZnFe_2O_4$ prepared at different temperatures (Fig. S6), SEM images of PMMA heated at 323, 373, 423, and 473 K (Fig. S7), and Arrott plot of the porous $Zn_{0.8}Ni_{0.2}Fe_2O_4$ (Fig. S8). This material is available free of charge on the web at http://www.csj.jp/journals/bcsj/.

References

1 a) R. C. Schroden, A. Stein, *Colloids and Colloid Assemblies* in *3D Ordered Macroporous Material*, ed. by F. Caruso, Wiley-VCH Verlag GmbH and Co., KGaA, Weinheim, Germany, **2004**, p. 465. b) A. Stein, R. C. Schroden, *Curr. Opin. Solid State Mater. Sci.* **2001**, *5*, 553. c) A. Stein, *Microporous Mesoporous Mater.* **2001**, *44–45*, 227.

2 H. Yan, C. F. Blanford, B. T. Holland, W. H. Smyrl, A. Stein, *Chem. Mater.* **2000**, *12*, 1134.

3 a) S. Sokolov, A. Stein, *Mater. Lett.* **2003**, *57*, 3593. b) H. Yan, S. Sokolov, J. C. Lytle, A. Stein, F. Zhang, W. H. Smyrl, *J. Electrochem. Soc.* **2003**, *150*, A1102. c) S. Sokolov, D. Bell, A. Stein, *J. Am. Ceram. Soc.* **2003**, *86*, 1481.

4 Y. Zhang, Z. Lei, J. Li, S. Lu, *New J. Chem.* **2001**, *25*, 1118.

5 a) H. Yan, C. F. Blanford, J. C. Lytle, C. B. Carter, W. H. Smyrl, A. Stein, *Chem. Mater.* **2001**, *13*, 4314. b) H. Yan, C. F. Blanford, W. H. Smyrl, A. Stein, *Chem. Commun.* **2000**, 1477.

6 F. Chen, C. Xia, M. Liu, *Chem. Lett.* **2001**, 1032.

7 a) Y. N. Kim, S. J. Kim, E. K. Lee, E. O. Chi, N. H. Hur, C. S. Hong, *J. Mater. Chem.* **2004**, *14*, 1774. b) E. C. Chi, Y. N. Kim, J. C. Kim, N. H. Hur, *Chem. Mater.* **2003**, *15*, 1929. c) Y. N. Kim, E. O. Chi, J. C. Kim, E. K. Lee, N. H. Hur, *Solid State Commun.* **2003**, *128*, 339.

8 M. Sadakane, T. Asanuma, J. Kubo, W. Ueda, *Chem. Mater.* **2005**, *17*, 3546.

9 M. Sadakane, C. Takahashi, N. Kato, T. Asanuma, H. Ogihara, W. Ueda, *Chem. Lett.* **2006**, *35*, 480.

10 a) D. Zou, S. Ma, R. Guan, M. Park, L. Sun, J. J. Aklonis, R. Salovey, *J. Polym. Sci., Part A: Polym. Chem.* **1992**, *30*, 137. b) J. C. Lytle, H. Yan, N. S. Ergang, W. H. Smyrl, A. Stein, *J. Mater. Chem.* **2004**, *14*, 1616.

11 K. Sasahara, T. Hyodo, Y. Shimizu, M. Egashira, *J. Eur. Ceram. Soc.* **2004**, *24*, 1961.

12 a) J. Smit, J. H. P. J. Wijn, *Ferrites*, Philips Technical Library, Eindhoven, Netherland, **1959**, p. 144. b) T. T. Srinivasan, P. Ravindranathan, L. E. Cross, R. Roy, R. E. Newnham, *J. Appl. Phys.* **1988**, *63*, 3789. c) C.-K. Kim, J.-H. Lee, S. Katoh, R. Murakami, M. Yoshimura, *Mater. Res. Bull.* **2001**, *36*, 2241. d) E. E. Sileo, R. Rotelo, S. E. Jacobo, *Physica B* **2002**, *320*, 257.

13 a) W. Dong, H. J. Bongard, B. Tesche, F. Marlow, *Adv. Mater.* **2002**, *14*, 1457. b) W. Dong, H. J. Bongard, F. Marlow, *Chem. Mater.* **2003**, *15*, 568.

14 a) Y. A. Vlasov, N. Yao, D. J. Norris, *Adv. Mater.* **1999**, *11*, 165. b) P. Jiang, K. S. Hwang, D. M. Mittleman, J. F. Bertone, V. L. Colvin, *J. Am. Chem. Soc.* **1999**, *121*, 11630.

15 a) J. E. G. J. Wijnhoven, W. L. Vos, *Science* **1998**, *281*, 802. b) A. Richel, A. N. P. Johnson, D. W. McComb, *Appl. Phys. Lett.* **2000**, *76*, 1816. c) J. E. G. J. Wijnhoven, L. Bechger, W. L. Vos, *Chem. Mater.* **2001**, *13*, 4486. d) D. Wang, F. Caruso, *Adv. Mater.* **2003**, *15*, 205.

16 B. T. Holland, C. F. Blandford, J. C. Lytle, C. B. Carter, W. H. Smyrl, A. Stein, *Chem. Mater.* **1999**, *11*, 795.

17 C. F. Blanford, H. Yan, R. C. Schroden, M. Al-Daous, A. Stein, *Adv. Mater.* **2001**, *13*, 401.

18 In the case of two spherical particles A and B, the diameter ratios (dA/dB) which form the octahedron AB_6 and tetrahedron AB_4 are about 0.42 and 0.23, respectively.

19 Assuming that the crystallites are spheres, the surface area could be calculated as Scal. $= 6/d \cdot x$, where x: crystallite size, d: density of $ZnFe_2O_4$ ($5.33\,g\,cm^{-3}$).

20 a) C. Caizer, M. Stefanescu, *J. Phys. D: Appl. Phys.* **2002**, *35*, 3035. b) M. Stefănescu, V. Sasca, M. Birzescu, *J. Therm. Anal. Calorim.* **1999**, *56*, 579.

21 The density of EG–methanol solution containing $Zn(NO_3)_2$ and $Fe(NO_3)_3$ (total metal concentration: 2 M) was $1.34\,g\,cm^{-3}$. The production of $ZnFe_2(C_2H_2O_4)_4$ and $ZnFe_2O_4$ corresponded to a weight loss of 74 and 88%, respectively.

22 Densities of EG–methanol solution containing $Zn(NO_3)_2$ and $Fe(NO_3)_3$ (total metal concentration: 2 M) and PMMA were, respectively, 1.34 and $1.2\,g\,cm^{-3}$. Assuming that all PMMA spheres were packed in fcc mode (26 vol % of the template have void space), nitrogen content was calculated to be ca. 1.6 wt %.

23 Curie temperature of the 3DOM $Zn_{0.8}Ni_{0.2}Fe_2O_4$ was determined to be 273 K (Fig. S8, Supporting Information), which is slightly lower than the reported value (310 K) for the same sample prepared by the conventional method.[12]